The Astrophysical Journal, 588:7–17, 2003 May 1

CLUSTER MORPHOLOGY AS A TEST OF DIFFERENT COSMOLOGICAL MODELS

Tamon Suwa and Asao Habe
Division of Physics, Graduate School of Science, Hokkaido University, Sapporo 060-0810, Japan; tamon@astro1.sci.hokudai.ac.jp, habe@astro1.sci.hokudai.ac.jp

Kohji Yoshikawa
Department of Astronomy, Kyoto University, Kyoto 606-8502, Japan; kohji@kusastro.kyoto-u.ac.jp

and

Takashi Okamoto
Yukawa Institute for Theoretical Physics, Kyoto University, Kyoto 606-8502, Japan; and Department of Physics, University of Durham, South Road, Durham DH1 3LE, England, UK; takashi.okamoto@durham.ac.uk
Received 2001 August 9; accepted 2003 January 6

ABSTRACT

We investigate how cluster morphology is affected by the cosmological constant in low-density universes. Using high-resolution cosmological N-body/smoothed particle hydrodynamics simulations of flat cold dark matter (ΛCDM; $\Omega_0 = 0.3,\ \lambda_0 = 0.7$) and open cold dark matter (OCDM; $\Omega_0 = 0.3,\ \lambda_0 = 0$) universes, we calculate statistical indicators to quantify the irregularity of the cluster morphologies. We study axial ratios, center shifts, cluster clumpiness, and multipole-moment power ratios as indicators for the simulated clusters at $z = 0$ and 0.5. Some of these indicators are calculated for both the X-ray surface brightness and projected mass distributions. In ΛCDM all these indicators tend to be larger than those in OCDM at $z = 0$. This result is consistent with the analytical prediction of Richstone, Loeb, & Turner, that is, clusters in ΛCDM are formed later than in OCDM and have more substructure at $z = 0$. We perform a Kolmogorov-Smirnov test on each indicator for these two models. We then find that the results for the multipole-moment power ratios and the center shifts for the X-ray surface brightness are under the significance level (5%). Our results also show that these two cosmological models can be distinguished more clearly at $z = 0$ than at $z = 0.5$ by these indicators.

Subject headings: cosmological parameters — cosmology: theory — galaxies: clusters: general — methods: numerical

1. INTRODUCTION

Measurement of the cosmological parameters, such as the Hubble constant H_0, the density parameter Ω_0, and the cosmological constant Λ, is one of the most important studies in observational cosmology. From observational evidence, the density parameter Ω_0 is estimated to be around 0.3 (e.g., Bahcall et al. 1999). The inflationary cosmology requires $\Omega_0 + \lambda_0 = 1$, where $\lambda_0 = \Lambda/(3H_0^2)$, and is supported by recent observations of the cosmic microwave background (e.g., de Bernardis et al. 2000). Distant Type Ia supernovae (SNe Ia) are assumed to be standard candles to explore the effect of a cosmological constant by searching for evidence of accelerated expansion (Perlmutter et al. 1999; Riess et al. 1998). Several systematic uncertainties in the observational data of SNe Ia have been pointed out (Totani & Kobayashi 1999; Gibson et al. 2000). Therefore, independent studies in the nonlinear regime are important for confirming the values of the cosmological parameters.

Richstone, Loeb, & Turner (1992) proposed that the fraction of clusters that have significant substructure can be a probe of the density parameter Ω_0, since the fraction of recently formed clusters strongly depends on Ω_0 and such young clusters are likely to have substructure. They have also revealed that the formation epoch of clusters in a universe with a cosmological constant is later than that in a universe without a cosmological constant, although the effect of the cosmological constant is much smaller than that of the density parameter. In fact, Wilson, Cole, & Frenk (1996) showed that the statistics of the quadrupoles of the column mass density of clusters strongly depends on the value of Ω_0, while it is quite insensitive to the value of λ_0.

Some authors have studied whether or not cosmological models with and without a cosmological constant can be discriminated by the statistics of the irregularity of cluster morphologies (Jing et al. 1995; Crone, Evrard, & Richstone 1996; Buote & Xu 1997). They performed pure N-body simulations in low-density flat universes ($\Omega_0 = 0.2$–0.35, $\lambda_0 = 1 - \Omega_0$) and open universes ($\Omega_0 = 0.2$–$0.35,\ \lambda_0 = 0$). Jing et al. (1995) and Crone et al. (1996) quantified morphologies of the X-ray surface brightness of clusters from N-body results assuming hydrostatic equilibrium of hot gas in the gravitational potentials of the clusters. Using a Kolmogorov-Smirnov (K-S) test, they showed that a low-density flat universe and an open universe are distinguishable from each other by the center shifts. On the other hand, Buote & Xu (1997) obtained multipole-moment power ratios for clusters in their N-body simulations and compared those in a low-density flat universe and those in an open universe. They concluded that these two cosmological models are not distinguishable by the multipole power ratios. Since these authors estimated the hot-gas distribution from N-body simulations, their results are in question, and thus simulations including hydrodynamics are desired.

In previous hydrodynamic simulations (Evrard et al. 1993; Mohr et al. 1995), the numbers of clusters were not enough to perform a statistical comparison. Although Valdarnini, Ghizzardi, & Bonometto (1999) analyzed a

sufficient number of clusters for various cosmological models, the effect of the tidal field from larger scales ($\gtrsim$30–50 h^{-1}Mpc) was neglected in their simulations because they performed tree–smoothed particle hydrodynamic (tree-SPH) simulations of individual clusters selected from the large N-body simulations. By comparing the simulated clusters and the *ROSAT* X-ray cluster data, they pointed out that a statistical test for the observed data favors the high-density ($\Omega_0 = 1$; standard cold dark matter [SCDM]) model rather than the *concordant* low-density flat ($\Omega_0 = 0.3$, $\lambda_0 = 0.7$) model. It is worthwhile to confirm their results with simulations that take account of the tidal field from outside the clusters. We thus simulate comoving 150 h^{-1} Mpc boxes with a particle-particle-particle-mesh (P^3M) SPH code.

In this paper, we study the morphologies of simulated clusters in flat cold dark matter (ΛCDM; $\Omega_0 = 0.3$, $\lambda_0 = 0.7$) and open cold dark matter (OCDM; $\Omega_0 = 0.3$, $\lambda_0 = 0$) universes by using high-resolution simulations. We perform large simulations to obtain a sufficient number of clusters for statistical comparisons. The reason why we study the difference between low-density universes despite the fact that recent cosmic microwave background (CMB) data (e.g., de Bernardis et al. 2000) support a flat universe is as follows. As we mentioned above, the irregularity of cluster morphologies is quite sensitive to the value of Ω_0, while it is rather insensitive to the value of λ_0. Thus, the statistical indicators that can discriminate between the low-density models with and without the cosmological constant λ_0 enable us to detect small differences in the formation histories of clusters in different but similar cosmologies, such as a low-density universe with a time-dependent vacuum energy. Furthermore, because the CMB data provide us only with information about the linear density fluctuations, the consistency test in the nonlinear regime is very important. For instance, if the finding of Valdarnini et al. (1999) is true, we should consider what causes the discrepancy. Unfortunately, the resolution in our simulations is not sufficient for making a direct comparison with high-resolution X-ray observations by *Chandra* or *XMM-Newton*, and our simulations do not include some important physical processes such as cooling and heating, which may affect the morphology of the X-ray surface brightness. Therefore, here we restrict ourselves to finding effective statistical indicators for discriminating between two low-density universes, and we do not compare our simulation results with observations.

We identify clusters in our simulation and calculate various statistical indicators for them. The K-S tests are performed to measure how effectively these indicators distinguish between these two cosmological models. These indicators are calculated for the projected mass density as well as the X-ray surface brightness of clusters of galaxies. The X-ray surface brightness reflects the distribution of hot gas in the cluster. On the other hand, the projected mass density is dominated by the distribution of dark matter. Although dark matter cannot be observed directly, a method by which the mass distribution is reconstructed from small-distortion images of background galaxies caused by gravitational lensing (these small distortions are called the "weak-shear field") has been developed recently (e.g., Mellier 1999; Luppino & Kaiser 1997; Clowe et al. 2000). The precision of this method is not yet sufficient to probe cluster substructure. It is, however, likely that this mass reconstruction method will progress and become a useful tool for measuring substructure in galaxy clusters. Schneider & Bartelmann (1997) have already investigated the possibility of deriving multipole moments of the projected mass distribution of clusters with weak lensing.

The organization of this paper is as follows: In § 2 we describe the numerical simulations used in this paper, the method of cluster identification, and the definitions of the indicators that we use. We give the mean values and standard deviations of the indicators for simulated clusters and show the results of the K-S tests on these indicators in § 3. In § 4 we discuss our results and present our conclusion.

2. METHOD

2.1. *Numerical Simulations*

Our simulations are based on a P^3M-SPH algorithm. A detailed description of our simulation method is given in Yoshikawa, Jing, & Suto (2000).

We use two cosmological models, OCDM and ΛCDM. Cosmological parameters in the two models, except for the cosmological constant, are as follows: the Hubble constant in units of 100 km s^{-1} Mpc^{-1}, $h = 0.7$, the density parameter $\Omega_0 = 0.3$, the baryon density parameter $\Omega_b = 0.015\ h^{-2}$, the rms density fluctuation amplitude on a scale of 8 h^{-1} Mpc, $\sigma_8 = 1.0$, and the power-law index of the primordial density fluctuations, $n = 1.0$. The normalized cosmological constant λ_0 is 0 and 0.7 for OCDM and ΛCDM, respectively. The simulation of ΛCDM is the same as L150A in Yoshikawa et al. (2000), and that of OCDM is carried out in this paper.

Each simulation employs $N_{\rm DM} = 128^3$ dark matter particles and the same number of SPH particles. The masses of a dark matter particle and an SPH particle are 1.7×10^{11} and $2.0 \times 10^{10}\ M_\odot$, respectively. The size of the comoving simulation box, $L_{\rm box}$, is 150 h^{-1} Mpc, and the box has periodic boundary conditions. We use a spline (S2) gravitational softening (Hockney & Eastwood 1981), and the softening length $\epsilon_{\rm grav}$ is set to be $L_{\rm box}/(10N_{\rm DM}^{1/3})$ ($\sim$120 h^{-1} kpc). The smoothing length of each SPH particle is determined by

$$h_i^{(n)} = \frac{1}{2}\left[1 + \left(\frac{N_s}{N_i^{(n-1)}}\right)^{1/3}\right] h_i^{(n-1)}\ , \qquad (1)$$

where $h_i^{(n)}$ is the smoothing length of the ith particle at the nth time step, $N_i^{(n)}$ is the number of neighbor particles of the ith particle at the nth time step (the number of particles inside a sphere of radius $h_i^{(n)}$), and N_s is mean number of neighbor particles (Hernquist & Katz 1989). We set $N_s = 32$ and the minimum SPH smoothing length as $h_{\rm min} = \epsilon_{\rm grav}/4$ ($\sim$30 h^{-1} kpc). We use the COSMICS package (Bertschinger 1995) to generate initial conditions at $z = 25$. Our simulations are carried out on a VPP5000, and each run takes about 50 hr using 8PE with parallel P^3M-SPH. The memory resource needed to run each simulation is 500 MB.

We calculate statistical indicators for the clusters in our simulations at $z = 0.5$ and 0. The reason for this is that the formation rate of galaxy clusters in ΛCDM is expected to exceed that in OCDM for $z < 0.8$ as shown in Figure 1, which shows the formation rate of galaxy clusters as a function of redshift according to the analytical formula given by Richstone et al. (1992). In Figure 1 the number of formed clusters is normalized by the present value, and the cosmic

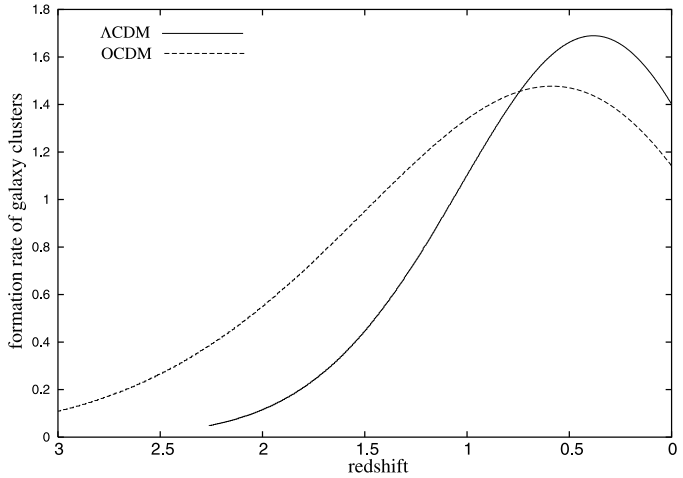

FIG. 1.—Formation rate of galaxy clusters. *Solid curve*: Formation rate in ΛCDM. *Dashed curve*: Formation rate in OCDM.

time is also normalized by the present age of the universe. The solid and dashed curves indicate the formation rates in ΛCDM and in OCDM, respectively. Since just before $z = 0.5$ the formation rate in ΛCDM exceeds that in OCDM, we expect that the difference due to the cosmological constant can already be detected at $z = 0.5$. Moreover, mass reconstruction based on observations of the weak-shear field has an advantage for high-redshift clusters rather than nearby clusters, in principle.

2.2. *Cluster Identification*

Galaxy clusters are identified in the following way (Jing & Fang 1994; Thomas et al. 1998):

1. We pick up SPH particles whose gas densities are more than 200 times the background (gas and dark matter) density. Here, we define the "gas density of an SPH particle" as the gas density at the position of the SPH particle. The processes in steps 2 and 3 are performed for these selected particles.
2. We perform a friends-of-friends method (FOF; e.g., Davis et al. 1985) for the dense SPH particles selected in step 1. The linking length l is defined as $b\bar{n}^{-1/3}$, where $\bar{n}$ is mean number density of all SPH and dark matter particles in the simulation box, and the constant parameter $b = 0.5$. It should be noted that the dense SPH particles are confined within small-scale areas. Since the typical distance between these areas is significantly larger than $l\ (=b\bar{n}^{-1/3})$, the number of groups found by FOF does not depend on b strongly. We confirm that both the number of the groups found in this step and the number of clusters found in the following steps are not so different for $0.2 \leq b \leq 1.0$.
3. The densest SPH particle in each group is defined as a "core" particle of the group.
4. We draw a sphere of which the center is on the position of the core and seek a radius in which the mean density of total matter is 200 times the background density of total matter. This radius is called r_{200}.
5. If the total mass in the sphere with radius r_{200} is more than $2 \times 10^{14}\ h^{-1}\ M_{\odot}$, a set of particles in the sphere is a candidate for being a cluster of galaxies.

TABLE 1
NUMBER OF CLUSTERS FOR EACH MODEL AND REDSHIFT

Model	$z = 0$	$z = 0.5$
ΛCDM.....	66	28
OCDM	74	38

6. If another core particle exists in the sphere, the set that belongs to the less dense core is removed from the cluster-candidate list.

The candidates that are not removed are finally identified as clusters of galaxies. We define the center of a cluster by the position of the core particle. We find that this position is very close to the particle having the minimum gravitational potential in the cluster and that the distance between the core particle and the potential minimum is at most several tens of kiloparsecs in our simulation. We also find that the position of the core is close to the center of mass of the cluster, except for some clusters that have large substructures.

Figure 2 shows the mass distribution of the clusters. The top panel describes the distribution in ΛCDM, and the bottom one describes the distribution in OCDM. The solid line indicates the number of clusters at $z = 0$, and the dashed line indicates the number at $z = 0.5$. The maximum masses of clusters are $2.7 \times 10^{15}\ h^{-1}\ M_{\odot}$ (ΛCDM; $z = 0$), $9.3 \times 10^{14}\ h^{-1}\ M_{\odot}$ (ΛCDM; $z = 0.5$), $2.7 \times 10^{15}\ h^{-1}\ M_{\odot}$ (OCDM; $z = 0$), and $1.2 \times 10^{15}\ h^{-1}\ M_{\odot}$ (OCDM; $z = 0.5$). Table 1 shows the number of clusters found in each model. The number of clusters increases from $z = 0.5$ to $z = 0$. Table 2 shows the ratio of the mass inside clusters to the total mass in the simulation box. These ratios in both models are similar at $z = 0$, but the ratio in ΛCDM is smaller than that in OCDM at $z = 0.5$. This is consistent with the fact that ΛCDM clusters form later than OCDM clusters.

2.3. *Calculation of Column Density and X-Ray Surface Brightness*

Two of the indicators that we use in this paper, the center shifts and the power ratios, are calculated for X-ray surface brightness and the projected mass density for simulated clusters. Our numerical projection method from three dimensions to two dimensions is as follows.

First, for each cluster we prepare a cube centered on a core particle, and the sides of the cube are set to $2r_{200}$. The total number of grid points in the cube is 128^3. Each grid point is assigned indices (i, j, k), and this point is expressed by $\boldsymbol{r}_{ijk}$. We calculate the gas density and temperature at each grid point from SPH particles in this cube. The gas density

TABLE 2
RATIOS OF THE MASS INVOLVED IN THE CLUSTERS TO THE TOTAL MASS IN EACH SIMULATION

Model	$z = 0$ (%)	$z = 0.5$ (%)
ΛCDM.....	10.2	3.64
OCDM	11.4	5.21

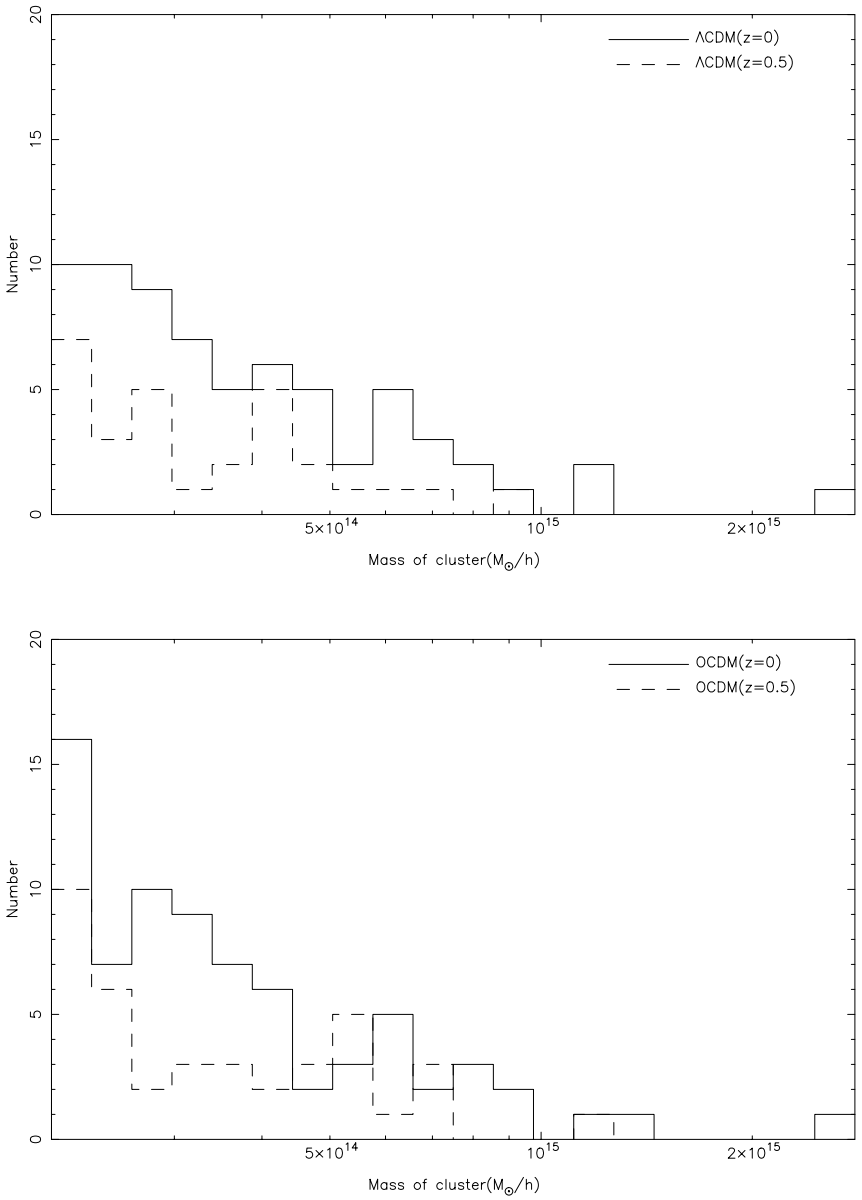

FIG. 2.—Mass distribution of the clusters. *Top*: Distribution in ΛCDM. *Bottom*: Distribution in OCDM. *Solid lines*: Number of clusters at $z = 0$. *Dashed lines*: Number at $z = 0.5$.

$\rho_{\rm gas}$ and temperature T at a grid point $\boldsymbol{r}_{ijk}$ are given by

$$\rho_{\rm gas}(\boldsymbol{r}_{ijk}) = \sum_s W\left(\frac{r_{s;ijk}}{h_s}\right)\frac{m_s}{h_s^3} \ , \tag{2}$$

$$T(\boldsymbol{r}_{ijk}) = \sum_s \frac{(\gamma-1)\mu m_p}{k_{\rm B}} W\left(\frac{r_{s;ijk}}{h_s}\right) u_s \ , \tag{3}$$

where h_s, m_s, u_s, and $r_{s;ijk}$ are the sth particle's smoothing length, mass, specific energy, and distance to the grid point ($r_{s;ijk} = |\boldsymbol{r}_{ijk} - \boldsymbol{r}_s|$, where $\boldsymbol{r}_s$ is the position of the sth particle), respectively. The function $W(t)$ is an SPH kernel, which is defined as

$$W(t) \equiv \frac{1}{\pi}\begin{cases} 1 - \dfrac{3}{2}t^2 + \dfrac{3}{4}t^3 \ , & 0 \le t \le 1 \ , \\ \dfrac{(2-t)^3}{4} \ , & 1 \le t \le 2 \ , \\ 0 \ , & \text{otherwise} \ . \end{cases}$$

We assume the specific heat ratio $\gamma = 5/3$ and the mean molecular mass $\mu = 0.6$. The smoothing length of an SPH particle is calculated in the usual way of the SPH method (Hernquist & Katz 1989; Monaghan 1992).

In order to obtain the mass density at each grid point from dark matter particles in each cluster, we use an interpolation technique, as in the previous SPH method. The smoothing length of each dark matter particle is set in order that each dark matter particle has 32 ± 3 neighbors.

The column density σ is derived from the projection of the total mass density $\rho_{\rm DM} + \rho_{\rm gas}$, where $\rho_{\rm DM}$ is the dark matter density and $\rho_{\rm gas}$ is the gas density. The X-ray surface brightness $\Sigma_{\rm X}$ is derived from the projection of $\rho_{\rm gas}^2 T^{1/2}$.

2.4. *Statistical Indicators*

We calculate statistical indicators for each cluster of galaxies to quantify the substructure and perform the K-S tests. As statistical indicators, we adopt the axial ratio, the

$M_{\rm int}$, the multipole-moment power ratio, and the center shift. The definitions are described below.

2.4.1. *Axial Ratio*

The axial ratio is an indicator for showing the deviation from sphericity of a cluster of galaxies (Dutta 1995; Jing et al. 1995; Thomas et al. 1998). In a coordinate system whose origin is at the center of mass of the cluster, the following tensor's eigenvalues are calculated for all dark matter particles and SPH particles:

$$I_{ij} = \sum_s m_s x_i x_j \ . \tag{4}$$

These eigenvalues are labeled λ_1, λ_2, and λ_3 in decreasing order. If a cluster is an ellipsoid, its axial ratio is obtained by $(\lambda_1/\lambda_3)^{1/2}$.

2.4.2. $M_{\rm int}$

We use $M_{\rm int}$ as an indicator of clumpiness of clusters. We calculate $M_{\rm int}$ in a similar way to Thomas et al. (1998). For each cluster we perform an FOF method for all dark matter particles and SPH particles with initial linking length $l = \bar{n}_c^{-1/3}$, where $\bar{n}_c$ is the mean number density of dark matter and SPH particles in the cluster. Next, l is gradually lowered until it becomes $(100\bar{n}_c)^{-1/3}$. This causes the cluster to break up into several subclumps. At each stage, $M_{\rm int}$ is defined as

$$M_{\rm int} = \frac{m_1 + m_2 + m_3}{m_1} \ , \tag{5}$$

where $m_1 \geq m_2 \geq m_3$ are the masses of the three largest clumps. We use the maximum value of $M_{\rm int}$ as a measure of the clumpiness of the cluster.

2.4.3. *Center Shift*

The center shift measures major deviations from symmetry in the cluster mass distribution (Jing et al. 1995; Crone et al. 1996). We calculate the center shift for each cluster in a slightly different way from Jing et al. (1995). We first search for a peak value $c_{\rm peak}$ of σ or $\Sigma_{\rm X}$ in the cluster. The lowest contour level $c_{\rm lowest}$ is defined as the mean value of σ or $\Sigma_{\rm X}$ at $0.5r_{200}$. Next, the ith contour level is given as $c_i \equiv c_{\rm peak}(c_{\rm lowest}/c_{\rm peak})^{i/n_{\rm cont}}$, where $n_{\rm cont}$ is the total number of contours.

The center shift C is defined as

$$C = \sum_{i=1}^{n_{\rm cont}} w_i \left[(x_i - \bar{x})^2 + (y_i - \bar{y})^2 \right] \ , \tag{6}$$

where (x_i, y_i) is the center of the ith contour, $\bar{x} = \sum_i w_i x_i$, and $\bar{y} = \sum_i w_i y_i$. The weight of each contour, w_i, is proportional to the surface integral of σ or $\Sigma_{\rm X}$ in the region between this contour and the adjacent outer contour. The center shift shows the emission-weighted dispersion of the centers of contours. If a cluster has a great deal of substructure, then the outer contour's center is expected to shift from $(\bar{x}, \bar{y})$, and the center shift becomes large.

2.4.4. *Power Ratio*

The power ratios quantify the shape of projected cluster potentials and are derived from their multipole expansions (e.g., Buote & Tsai 1995, 1996; Tsai & Buote 1996; Buote 1998; Valdarnini et al. 1999).

The two-dimensional potential $\Psi(R, \phi)$ and column density $\sigma(R, \phi)$ are related by Poisson's equation,

$$\nabla^2 \Psi(R, \phi) = \sigma(R, \phi) \ , \tag{7}$$

where R and ϕ are projected polar coordinates about the center of mass of the cluster, and we ignore the constant factor in equation (7). The multipole expansion of $\Psi(R, \phi)$, which relies on the distribution of the material interior to R (e.g., Buote & Tsai 1995) is

$$\Psi(R, \phi) = -a_0 \ln\left(\frac{1}{R}\right) - \sum_{m=1}^{\infty} \frac{1}{mR^m} \times (a_m \cos m\phi + b_m \sin m\phi) \ , \tag{8}$$

where a_m and b_m are defined as follows:

$$a_m = \int_{R' \leq R} \sigma(\boldsymbol{x}')(R')^m \cos m\phi' \, d^2\boldsymbol{x}' \ , \tag{9}$$

$$b_m = \int_{R' \leq R} \sigma(\boldsymbol{x}')(R')^m \sin m\phi' \, d^2\boldsymbol{x}' \ , \tag{10}$$

where $\boldsymbol{x}' = (R', \phi')$. The mth moment power P_m is defined by integration of the square of the mth term of the multipole expansion (eq. [8]) over the boundary of a circular aperture of radius $R_{\rm ap}$:

$$P_m = \frac{1}{2m^2 R_{\rm ap}^{2m}} \left(a_m^2 + b_m^2\right) \ , \tag{11}$$

for $m > 0$, and

$$P_0 = a_0^2 \ , \tag{12}$$

for $m = 0$.

The moment power depends on not only the irregularity of the potential shape but also the magnitude of σ. Thus, we use the moment power ratio P_m/P_0 as an indicator of a cluster's irregularity. We define the unit of R, the radius in polar coordinates, as r_{200}, so that the power ratio is independent of the size of the cluster. Since the origin of the polar coordinates is the center of mass of the cluster, the dipole moment P_1 vanishes. The higher order ($m > 4$ in this paper) terms are affected by minor irregularities in cluster shapes; hence, we calculate the power ratio only for $m = 2$, 3, and 4. Because the power ratios depend on $R_{\rm ap}$ (Buote & Xu 1997; Valdarnini et al. 1999), we calculate the power ratios for some different values of $R_{\rm ap}$.

We also use the same definition of the power ratio for $\Sigma_{\rm X}$ by replacing σ with $\Sigma_{\rm X}$ in equations (9) and (10).

3. RESULTS

According to the analytical results of Richstone et al. (1992), the typical formation epoch of galaxy clusters in ΛCDM is delayed to a lower redshift than that in OCDM. This delay clearly appears at low z ($z \lesssim 0.8$–0.7, as shown in Fig. 1). We then calculate the indicators described in § 2 at $z = 0$ and $z = 0.5$ and perform the K-S test for each set of indicators obtained for the two cosmological models. The K-S test can be used as a statistical test to estimate the ability of an indicator to be used to discriminate between a model with and without λ_0. The result of the K-S test is the probability of the null hypothesis that two distributions of

TABLE 3
MEAN VALUES OF THE AXIAL RATIO

Redshift	ΛCDM	OCDM
$z = 0$	1.608	1.585
$z = 0.5$	1.644	1.696

the indicator are generated from the same population (Press et al. 1988). The significance level of the K-S test adopted in this paper is 5%. If the result of the K-S test for an indicator is under this level, we regard it as being able to distinguish between the two cosmological models by using this indicator.

3.1. *Axial Ratio*

The mean values of the axial ratios are shown in Table 3. From $z = 0.5$ to $z = 0$, the axial ratios decrease. At $z = 0$, the axial ratio in ΛCDM is larger than that in OCDM. This suggests that the clusters in ΛCDM have more substructure than those in OCDM, as expected from the analytical prediction.

The results of the K-S tests for the axial ratios are 0.495 for $z = 0$ and 0.661 for $z = 0.5$. Both are over the significance level (5%). Thus, the axial ratio is not useful for distinguishing between these two cosmological models.

Jing et al. (1995) performed K-S tests for the axial ratios, which were obtained in a slightly different way from ours, and the result of their K-S test is under the significance level (0.13×10^{-2}). In their calculations of the principal axes and axial ratios, they take, first, all particles within the virial radius of a cluster. They then calculate new principal axes and axial ratios using particles within an ellipsoid with the principal axes and axial ratios just determined. They repeat the same calculation for the updated ellipsoid until the axial ratios converge. We also calculate axial ratios by their method and perform a K-S test on them. In contrast with their result, the result of our K-S test is over the significance level (0.150 for $z = 0$ and 0.750 for $z = 0.5$), although our resolution is similar to theirs. The reason for this difference is unclear.

3.2. $M_{\rm int}$

The mean values of $M_{\rm int}$ are shown in Table 4. The value of $M_{\rm int}$ in ΛCDM is larger than that in OCDM at $z = 0$.

The results of the K-S tests for $M_{\rm int}$ are 0.770 for $z = 0$ and 0.192 for $z = 0.5$. Both of these are over the significance level. Again, we cannot use this indicator to distinguish between these two cosmological models.

The mean values and the results of the K-S tests are consistent with those of Thomas et al. (1998).

TABLE 4
MEAN VALUE OF $M_{\rm int}$

Redshift	ΛCDM	OCDM
$z = 0$	1.289	1.188
$z = 0.5$	1.284	1.189

TABLE 5
MEAN VALUES OF THE LOGARITHMS OF THE CENTER SHIFTS

Model (1)	$n_{\rm cont}$ (2)	$\log(C_\sigma)$ (3)	$\log(C_{\Sigma_{\rm X}})$ (4)
ΛCDM ($z = 0$).....	4	-2.65 ± 0.72	-3.43 ± 0.78
	5	-2.52 ± 0.69	-3.31 ± 0.82
	6	-2.43 ± 0.67	-3.26 ± 0.80
	7	-2.38 ± 0.64	-3.22 ± 0.80
	8	-2.33 ± 0.63	-3.20 ± 0.77
OCDM ($z = 0$)	4	-2.80 ± 0.70	-3.64 ± 0.75
	5	-2.72 ± 0.66	-3.56 ± 0.77
	6	-2.62 ± 0.67	-3.49 ± 0.75
	7	-2.59 ± 0.63	-3.47 ± 0.76
	8	-2.54 ± 0.62	-3.46 ± 0.76
ΛCDM ($z = 0.5$).....	4	-2.87 ± 0.58	-3.73 ± 0.67
	5	-2.71 ± 0.60	-3.62 ± 0.64
	6	-2.67 ± 0.57	-3.53 ± 0.64
	7	-2.63 ± 0.55	-3.49 ± 0.67
	8	-2.59 ± 0.55	-3.45 ± 0.64
OCDM ($z = 0.5$).....	4	-2.99 ± 0.68	-3.68 ± 0.77
	5	-2.89 ± 0.70	-3.59 ± 0.80
	6	-2.77 ± 0.68	-3.53 ± 0.76
	7	-2.73 ± 0.70	-3.46 ± 0.76
	8	-2.68 ± 0.69	-3.41 ± 0.80

NOTES.—Col. (1): Cosmological model and redshift. Col. (2): Number of contours. Cols. (3) and (4): Mean value of $\log(C)$ for the column density and the X-ray surface brightness, respectively.

3.3. *Center Shift*

The mean values and the standard deviations of the logarithm of the center shifts are shown in Table 5. The number of the contours, $n_{\rm cont}$, is varied from 4 to 8 to investigate the effect of the number of the contours. For large $n_{\rm cont}$, i.e., a small interval of contour level, C is large. In the case of a small interval, the center shift easily shows small substructures near to the center of the cluster.

The center shifts for σ, C_σ, are significantly larger than those for $\Sigma_{\rm X}$, $C_{\Sigma_{\rm X}}$. The shapes of the $\Sigma_{\rm X}$ contours reflect the distribution of the gas. Gas in a cluster relaxes more quickly than the collisionless dark matter (Frenk et al. 1999). This is the reason why the shapes of the $\Sigma_{\rm X}$ contours become rounder than those of σ and the center shifts for $\Sigma_{\rm X}$ become smaller than those for σ.

The center shifts in ΛCDM are larger than those in OCDM at the same redshift. This result reflects that the formation epoch of clusters in ΛCDM is later than in OCDM.

Figure 3 shows the result of the K-S tests for the center shifts. The top panel describes the results for the center shifts for the column density, and the bottom one describes the results for the X-ray surface brightness. In Figure 3, the dotted lines indicate the significance level (5%), the asterisks indicate the results at $z = 0$, and the circles indicate the results at $z = 0.5$. Using the center shifts for $\Sigma_{\rm X}$ at $z = 0$, we can distinguish between the two cosmological models in this range of the number of contours. The effect of contour level interval is not very significant for the K-S test.

In order to study the effect of the lowest level of contour, we also calculate the center shifts for $\Sigma_{\rm X}$ and σ in the two cases for which the lowest contour level is the mean value at $0.4r_{200}$ and $0.7r_{200}$. For the case of $0.7r_{200}$, the results of the K-S tests are over the significance level, except for one case with $C_{\Sigma_{\rm X}}$ ($z = 0$, $n_{\rm cont} = 8$). For the case of $0.4r_{200}$,

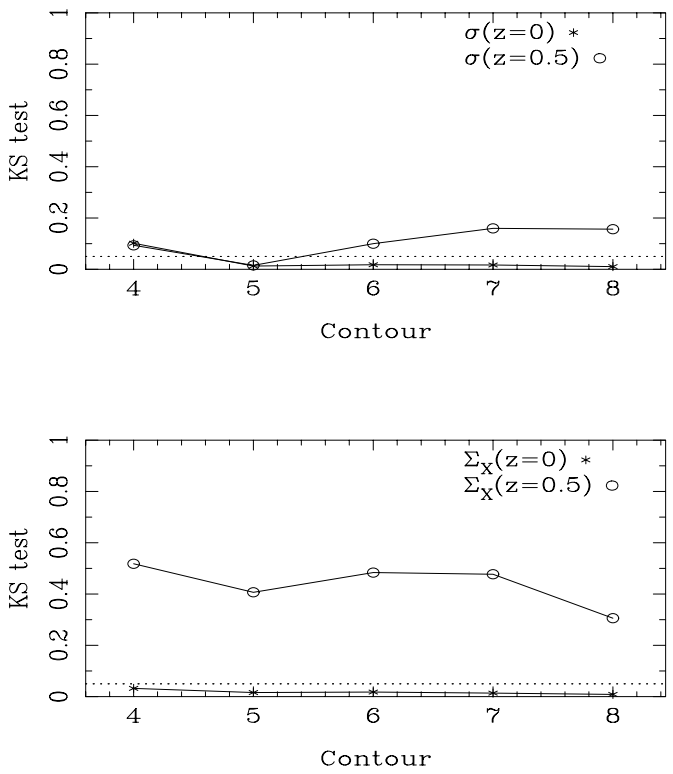

FIG. 3.—Results of the K-S tests for center shifts as a function of the number of contours. *Asterisks*: Results at $z = 0$. *Circles*: Results at $z = 0.5$. *Dotted line*: Significance level (5%).

the results are similar to the case of the lowest level at $0.5r_{200}$. We conclude that the center shift within $\sim 0.5r_{200}$ is a useful tool for clarifying the presence of a cosmological constant.

3.4. *Power Ratio*

We calculate the power ratios for various $R_{\rm ap}$ (0.4, 0.5, 0.6, 0.8, and 1.0 times r_{200}) in order to study how $R_{\rm ap}$ affects the result of the K-S test. We show the mean values and the standard deviations of the logarithm of the power ratios in Tables 6 and 7 for the column density and the X-ray surface brightness, respectively.

For small $R_{\rm ap}$ the power ratios are large, as shown in Tables 6 and 7. The most likely explanation of this property is that the power ratios for small $R_{\rm ap}$ readily reflect the small substructures around the cluster center.

We also calculate the power ratios for constant $R_{\rm ap}$, e.g., 0.4 and 0.6 h^{-1} Mpc. As shown in Table 8, the power ratios for the constant $R_{\rm ap}$ are smaller than the proportional $R_{\rm ap}$ case because the constant $R_{\rm ap}$ is less sensitive to the small substructures in small clusters than is the proportional $R_{\rm ap}$. In the constant $R_{\rm ap}$ case, the mean values and the standard deviations of the power ratios agree with Valdarnini et al. (1999).

From $z = 0.5$ to $z = 0$, the power ratios become smaller in both models. This is due to the fact that the fraction of relaxed clusters increases with time. Like the other indicators, the power ratios in ΛCDM are larger than those in OCDM at the same redshift, as expected.

Table 9 shows the results of the K-S tests for the power ratios for the column density, and Table 10 shows those for the X-ray surface brightness. The figures with asterisks in these tables are under the significance level (5%). Figures 4–6 show the results of the K-S tests summarized in Tables 9 and 10. At $z = 0$, we can distinguish between the two cosmological models by the power ratios for $\Sigma_{\rm X}$ for all $R_{\rm ap}$. Using the power ratios for σ for most $R_{\rm ap}$ except for P_3/P_0, we can also distinguish between the two cosmological models.

TABLE 6
MEAN VALUES OF $\log(P_m/P_0)$ FOR COLUMN DENSITY

Model (1)	$R_{\rm ap}$ (2)	$\log(P_2/P_0)$ (3)	$\log(P_3/P_0)$ (4)	$\log(P_4/P_0)$ (5)
ΛCDM ($z = 0$).....	$0.4r_{200}$	-2.90 ± 0.66	-4.38 ± 0.69	-4.89 ± 0.75
	$0.5r_{200}$	-2.94 ± 0.63	-4.52 ± 0.71	-4.91 ± 0.66
	$0.6r_{200}$	-2.98 ± 0.61	-4.61 ± 0.68	-4.96 ± 0.66
	$0.8r_{200}$	-3.05 ± 0.66	-4.63 ± 0.69	-5.05 ± 0.72
	$1.0r_{200}$	-3.15 ± 0.68	-4.70 ± 0.67	-5.20 ± 0.74
OCDM ($z = 0$)	$0.4r_{200}$	-3.03 ± 0.63	-4.58 ± 0.79	-5.11 ± 0.81
	$0.5r_{200}$	-3.09 ± 0.68	-4.63 ± 0.74	-5.11 ± 0.80
	$0.6r_{200}$	-3.15 ± 0.76	-4.61 ± 0.76	-5.10 ± 0.84
	$0.8r_{200}$	-3.20 ± 0.65	-4.72 ± 0.75	-5.22 ± 0.80
	$1.0r_{200}$	-3.29 ± 0.65	-4.85 ± 0.79	-5.36 ± 0.76
ΛCDM ($z = 0.5$).....	$0.4r_{200}$	-2.93 ± 0.69	-4.33 ± 0.67	-4.88 ± 0.69
	$0.5r_{200}$	-2.92 ± 0.51	-4.37 ± 0.58	-4.89 ± 0.65
	$0.6r_{200}$	-2.92 ± 0.50	-4.40 ± 0.57	-4.85 ± 0.66
	$0.8r_{200}$	-2.91 ± 0.51	-4.35 ± 0.51	-4.85 ± 0.67
	$1.0r_{200}$	-2.93 ± 0.51	-4.39 ± 0.63	-4.81 ± 0.64
OCDM ($z = 0.5$).....	$0.4r_{200}$	-2.76 ± 0.52	-4.29 ± 0.93	-4.78 ± 0.86
	$0.5r_{200}$	-2.78 ± 0.52	-4.38 ± 0.93	-4.75 ± 0.80
	$0.6r_{200}$	-2.80 ± 0.54	-4.40 ± 0.90	-4.79 ± 0.82
	$0.8r_{200}$	-2.87 ± 0.61	-4.43 ± 0.77	-4.90 ± 0.96
	$1.0r_{200}$	-3.02 ± 0.64	-4.44 ± 0.73	-5.02 ± 0.94

NOTES.—Col. (1): Cosmological models and redshifts. Col. (2): Aperture radius. Cols. (3)–(5): Mean values of the power ratios of the second, third, and fourth orders, respectively.

TABLE 7
MEAN VALUES OF $\log(P_m/P_0)$ FOR X-RAY SURFACE BRIGHTNESS

Model	R_{ap}	$\log(P_2/P_0)$	$\log(P_3/P_0)$	$\log(P_4/P_0)$
ΛCDM ($z = 0$).....	$0.4r_{200}$	-3.92 ± 0.96	-5.86 ± 1.14	-6.52 ± 1.31
	$0.5r_{200}$	-4.19 ± 0.99	-6.16 ± 1.14	-6.81 ± 1.32
	$0.6r_{200}$	-4.40 ± 1.01	-6.36 ± 1.22	-7.03 ± 1.34
	$0.8r_{200}$	-4.75 ± 1.05	-6.66 ± 1.32	-7.37 ± 1.41
	$1.0r_{200}$	-5.04 ± 1.09	-6.93 ± 1.40	-7.67 ± 1.49
OCDM ($z = 0$)	$0.4r_{200}$	-4.40 ± 0.97	-6.45 ± 1.29	-7.04 ± 1.42
	$0.5r_{200}$	-4.68 ± 1.03	-6.70 ± 1.39	-7.37 ± 1.59
	$0.6r_{200}$	-4.90 ± 1.05	-6.83 ± 1.40	-7.51 ± 1.58
	$0.8r_{200}$	-5.23 ± 1.12	-7.11 ± 1.55	-7.84 ± 1.70
	$1.0r_{200}$	-5.52 ± 1.15	-7.38 ± 1.60	-8.19 ± 1.76
ΛCDM ($z = 0.5$).....	$0.4r_{200}$	-3.54 ± 0.83	-5.41 ± 1.08	-5.99 ± 1.10
	$0.5r_{200}$	-3.79 ± 0.90	-5.64 ± 1.07	-6.30 ± 1.15
	$0.6r_{200}$	-3.97 ± 0.90	-5.79 ± 1.03	-6.50 ± 1.21
	$0.8r_{200}$	-4.28 ± 0.97	-6.04 ± 1.05	-6.74 ± 1.28
	$1.0r_{200}$	-4.50 ± 1.11	-6.08 ± 1.31	-6.76 ± 1.49
OCDM ($z = 0.5$).....	$0.4r_{200}$	-3.63 ± 1.16	-5.35 ± 1.53	-6.03 ± 1.64
	$0.5r_{200}$	-3.87 ± 1.20	-5.59 ± 1.59	-6.26 ± 1.75
	$0.6r_{200}$	-4.04 ± 1.21	-5.83 ± 1.66	-6.45 ± 1.79
	$0.8r_{200}$	-4.29 ± 1.35	-6.05 ± 1.77	-6.71 ± 2.05
	$1.0r_{200}$	-4.59 ± 1.40	-6.30 ± 1.87	-6.98 ± 2.08

4. DISCUSSION AND CONCLUSIONS

We have investigated the morphologies of galaxy clusters in ΛCDM and OCDM at $z = 0$ and $z = 0.5$ using large hydrodynamic simulations. For clusters in each model we have calculated the axial ratios, M_{int}, center shifts, and multipole-moment power ratios as statistical indicators that quantify the irregularity of cluster morphologies.

The power ratios and the center shifts are calculated for the projected density σ as well as the X-ray surface brightness Σ_X. For σ, both indicators show a larger value than those for Σ_X because the relaxation timescale of the collisionless particles is much longer than that of the collisional gas particles (Frenk et al. 1999; Valdarnini et al. 1999).

At $z = 0$ all mean values of statistical indicators in ΛCDM show larger values than those in OCDM. These large values, which indicate large irregularity of the clusters, suggest a more recent formation of the clusters in ΛCDM, as expected from the analytic prediction (Richstone et al. 1992) and previous numerical studies (Mohr et al. 1995; Crone et al. 1996; Buote & Xu 1997).

We use K-S tests to estimate the ability of the indicators to distinguish between two cosmological models. From the results of these K-S tests, the distributions of the axial ratios

TABLE 8
MEAN VALUES OF $\log(P_m/P_0)$ WITH CONSTANT R_{ap} FOR X-RAY SURFACE BRIGHTNESS

Model	R_{ap} (h^{-1} Mpc)	$\log(P_2/P_0)$	$\log(P_3/P_0)$	$\log(P_4/P_0)$
ΛCDM ($z = 0$).....	0.4	-5.65 ± 0.85	-7.66 ± 1.14	-8.22 ± 1.23
	0.6	-6.03 ± 0.93	-7.97 ± 1.23	-8.62 ± 1.32
	0.8	-6.39 ± 0.98	-8.39 ± 1.14	-8.98 ± 1.31
	1.0	-6.68 ± 1.02	-8.63 ± 1.24	-9.26 ± 1.34
	1.2	-6.90 ± 1.05	-8.81 ± 1.31	-9.52 ± 1.45
OCDM ($z = 0$)	0.4	-5.96 ± 0.89	-8.05 ± 1.20	-8.57 ± 1.29
	0.6	-6.47 ± 0.96	-8.55 ± 1.21	-9.09 ± 1.40
	0.8	-6.83 ± 1.05	-8.85 ± 1.39	-9.48 ± 1.58
	1.0	-7.12 ± 1.08	-9.07 ± 1.47	-9.74 ± 1.64
	1.2	-7.35 ± 1.12	-9.25 ± 1.56	-9.95 ± 1.70
ΛCDM ($z = 0.5$).....	0.4	-5.35 ± 1.04	-7.11 ± 1.46	-7.70 ± 1.43
	0.6	-5.78 ± 1.20	-7.57 ± 1.54	-8.22 ± 1.69
	0.8	-6.13 ± 1.28	-7.99 ± 1.40	-8.58 ± 1.80
	1.0	-6.36 ± 1.33	-8.17 ± 1.48	-8.68 ± 1.81
	1.2	-6.58 ± 1.43	-8.15 ± 1.62	-8.80 ± 1.91
OCDM ($z = 0.5$).....	0.4	-5.58 ± 1.21	-7.28 ± 1.64	-7.95 ± 1.74
	0.6	-6.05 ± 1.26	-7.89 ± 1.59	-8.48 ± 1.85
	0.8	-6.39 ± 1.35	-8.12 ± 1.75	-8.74 ± 2.03
	1.0	-6.70 ± 1.38	-8.44 ± 1.78	-9.14 ± 2.12
	1.2	-6.94 ± 1.39	-8.67 ± 1.80	-9.34 ± 1.99

TABLE 9
RESULTS OF THE K-S TESTS FOR THE POWER RATIOS FOR THE COLUMN DENSITY

P_m/P_0	R_{ap}	$z = 0$	$z = 0.5$
P_2/P_0.....	$0.4r_{200}$	2.43E−2*	4.45E−1
	$0.5r_{200}$	9.03E−2	4.57E−1
	$0.6r_{200}$	3.30E−2*	3.21E−1
	$0.8r_{200}$	1.38E−2*	6.84E−1
	$1.0r_{200}$	5.79E−3*	1.04E−1
P_3/P_0.....	$0.4r_{200}$	4.38E−2*	1.16E−1
	$0.5r_{200}$	1.23E−1	2.20E−1
	$0.6r_{200}$	3.37E−1	8.40E−2
	$0.8r_{200}$	4.28E−2*	4.87E−2*
	$1.0r_{200}$	1.24E−1	2.32E−1
P_4/P_0.....	$0.4r_{200}$	3.25E−2*	4.25E−1
	$0.5r_{200}$	1.40E−3*	3.60E−1
	$0.6r_{200}$	1.53E−2*	2.81E−1
	$0.8r_{200}$	1.43E−2*	1.36E−1
	$1.0r_{200}$	8.48E−2	8.97E−2

in the two cosmological models are indistinguishable. The distributions of $M_{\rm int}$ in ΛCDM and OCDM are also similar. Using the center shifts and the power ratios for Σ_X at $z = 0$, we can distinguish between the two cosmological models. It is possible to discriminate between ΛCDM and OCDM using the center shifts, P_2/P_0, and P_4/P_0 for σ at $z = 0$. At $z = 0.5$ we can distinguish between the two cosmological models by the power ratios for Σ_X but not by the center shifts for Σ_X or both the power ratios and the center shifts for σ.

Using the power ratios for Σ_X we can distinguish between ΛCDM and OCDM better than using those for σ, as shown in Tables 9 and 10. This may be due to the fact that the relaxation timescale of dark matter that dominates σ is longer than that of the gas on which Σ_X mainly depends, as described above. Since σ does not settle rapidly after the cluster formation epoch, the power ratios for σ are relatively insensitive to the difference of the cluster formation epochs.

We also note that the power ratios for Σ_X depend more on irregularities in high-density regions (i.e., in the central region) than those for σ because Σ_X is proportional to the square of gas density (and the square root of temperature) as $\rho_{\rm gas}^2 T^{1/2}$. Since small substructures that appear in the central region are expected to be erased more easily than large-scale substructures, the power ratios for Σ_X are probably

TABLE 10
RESULTS OF THE K-S TESTS FOR THE POWER RATIOS FOR THE X-RAY SURFACE BRIGHTNESS

P_m/P_0	R_{ap}	$z = 0$	$z = 0.5$
P_2/P_0.....	$0.4r_{200}$	4.19E−8*	1.03E−2*
	$0.5r_{200}$	7.20E−8*	1.47E−2*
	$0.6r_{200}$	1.33E−6*	2.70E−2*
	$0.8r_{200}$	1.47E−6*	2.99E−2*
	$1.0r_{200}$	2.56E−6*	3.30E−2*
P_3/P_0.....	$0.4r_{200}$	6.75E−6*	2.12E−1
	$0.5r_{200}$	3.51E−5*	1.42E−1
	$0.6r_{200}$	4.43E−5*	9.17E−3*
	$0.8r_{200}$	2.24E−3*	1.15E−3*
	$1.0r_{200}$	7.99E−4*	2.43E−3*
P_4/P_0.....	$0.4r_{200}$	2.06E−6*	1.79E−1
	$0.5r_{200}$	6.83E−5*	9.77E−2
	$0.6r_{200}$	4.72E−5*	3.22E−2*
	$0.8r_{200}$	2.52E−4*	1.28E−2*
	$1.0r_{200}$	7.56E−5*	2.68E−3*

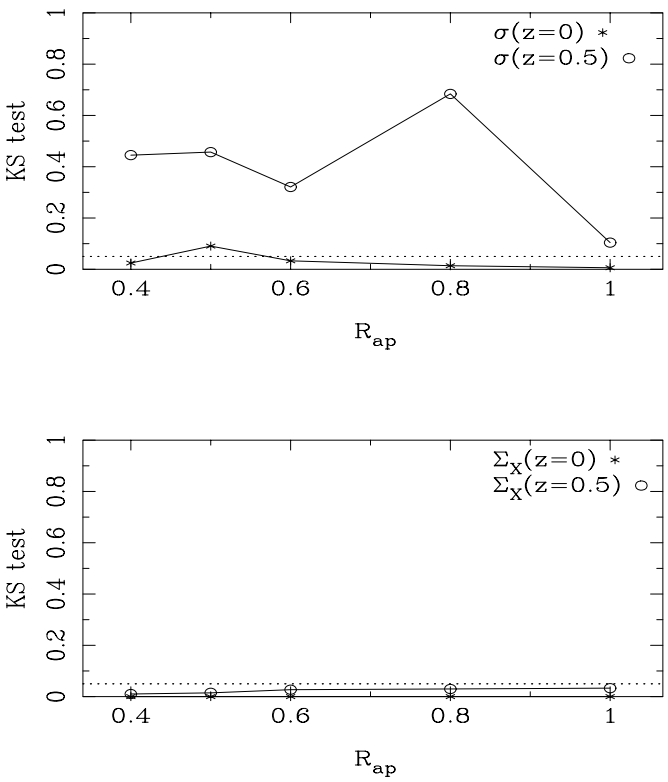

FIG. 4.—Same as Fig. 3, but for P_2/P_0

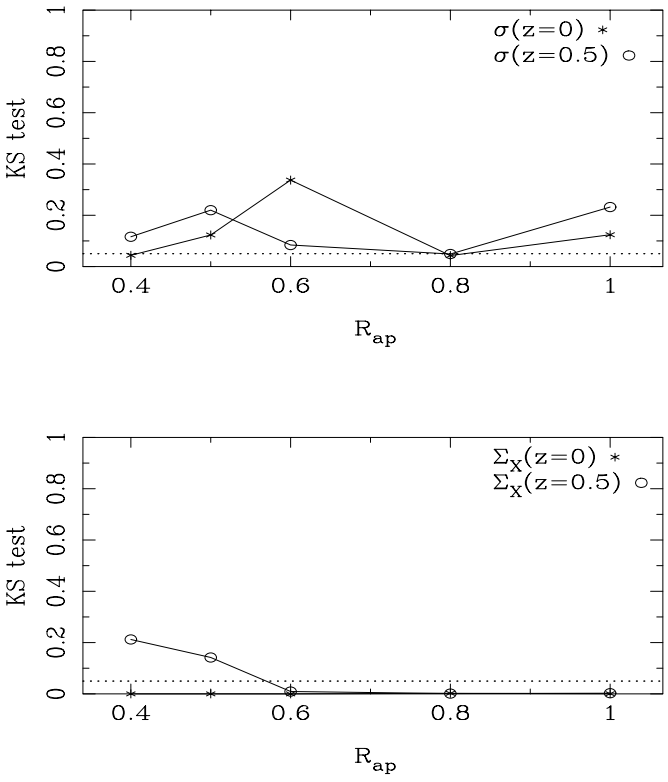

FIG. 5.—Same as Fig. 3, but for P_3/P_0

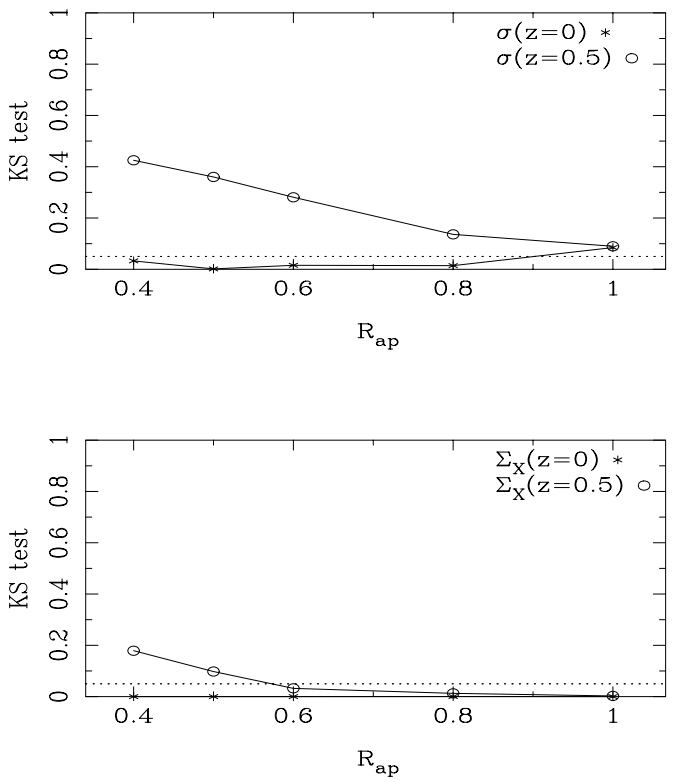

FIG. 6.—Same as Fig. 3, but for P_4/P_0

more sensitive to the cluster formation epoch than those for σ. In order to clarify this point, we calculate power ratios for σ^2 and then perform K-S tests. The results for σ^2 are better than those for σ but worse than those for Σ_X, reflecting the difference in relaxation timescale. From these facts, we suggest that indicators that focus on the central regions of clusters are suitable for distinguishing between ΛCDM and OCDM.

Some previous studies (Jing et al. 1995; Crone et al. 1996; Buote & Xu 1997) compared ΛCDM and OCDM by using pure N-body simulations in which they assume that $\rho_{\rm gas}$ is proportional to $\rho_{\rm DM}$. For clusters that are not well relaxed, however, this assumption may not be valid. Using the power ratios for Σ_X, Buote & Xu (1997) could not distinguish between ΛCDM and OCDM, while we can. On the other hand, Jing et al. (1995) and Crone et al. (1996) showed that ΛCDM and OCDM are distinguishable by using center shifts, and we also reach the same conclusion. These results suggest that the power ratios are more sensitive to the existence of gas than the center shifts.

Let us discuss differences in the properties of these two indicators. The center shifts show a large value when there are substructures whose sizes are large enough to shift a center of contour from the inner contour to the outer one. Since the center shifts are sensitive to large-size substructures that can be detected in the distributions of both gas and dark matter in the cluster, the center shifts for the simulations with and without gas are expected to be similar. In contrast, the power ratios are more sensitive to small-size substructures than the center shifts, and such small-size substructures are sometimes detected only in the dark matter distribution since corresponding gas structures are already relaxed. Hence, the difference between the power ratios for the simulations with and without gas is expected to be larger than that of the center shifts. In order to confirm this explanation, we calculate correlation coefficients of the power ratios for Σ_X and σ and those of center shifts for Σ_X and σ. As expected, the correlation coefficients of the power ratios tend to be smaller than those of the center shifts. Therefore, it is important to include a gas component in simulations in order to distinguish between the two cosmological models using the power ratios.

Although some authors (Evrard et al. 1993; Mohr et al. 1995) employed gas particles, the number of clusters was too small (eight clusters for each model). We use much larger size simulations ($L_{\rm box} = 150\ h^{-1}$ Mpc) than the previous studies in order to obtain a sufficient number of clusters to perform statistical tests (70–80 clusters at $z = 0$). The K-S test is significant when the number of samples is larger than 20 (Press et al. 1988).

Valdarnini et al. (1999) carried out hydrodynamic simulations for a sufficient number of clusters to perform statistical tests. By comparing their simulated clusters with *ROSAT* clusters, they showed that power ratios for gas in SCDM universes are in much better agreement with the *ROSAT* data than those for ΛCDM. Although this result is quite interesting, in order to give more conclusive results we should await *Chandra* and *XMM-Newton* data, which will have high resolutions and high signal-to-noise ratios, and much higher resolution simulations with additional important physical processes such as radiative cooling and SN feedback.

In comparison with the power ratios in ΛCDM obtained by Valdarnini et al. (1999), those obtained in this paper are systematically large. This difference results from the fact that $R_{\rm ap}$ for our power ratios is proportional to r_{200}, while $R_{\rm ap}$ in their paper was constant. Thus, our power ratios are more sensitive to small-scale irregularity for small clusters than theirs. Mean values of power ratios and their standard deviations in our simulations agree well with their results for the constant $R_{\rm ap}$ case.

Schuecker et al. (2001) showed that the fraction of clusters of galaxies with substructure is almost 50% for REFLEX+BCS clusters after correction for several systematic effects. They also suggested that the fraction of clusters with substructure depends on the number density of the clusters. Thus, this large fraction may be explained by the fact that a large fraction ($\sim$54% for $z \leq 0.1$) of rich clusters appear to belong to superclusters (Bahcall & Soneira 1984). On the other hand, the size of the simulation box of our and previous simulations may not be large enough for the realization of large superclusters, such as the Shapley supercluster, since the Shapley supercluster is expected to be formed from a 3.5 σ perturbation with a size of $\sim$30 Mpc (Ettori, Fabian, & White 1997). This may be the reason why the previous simulations of open and flat Λ universes do not agree with the *ROSAT* X-ray observation data. We will simulate initial conditions corresponding to the local universe to examine this possibility.

Our conclusion is as follows: The power ratios and the center shifts for Σ_X can be used to distinguish between ΛCDM and OCDM. Since the formation histories of clusters in ΛCDM are similar to those in OCDM compared with a high-density universe, these indicators will be powerful probes for testing these cosmological models in the nonlinear regime.

We are grateful to Vincent Eke for helpful advice. We also thank the anonymous referee for valuable comments. Numerical computation in this work was carried out on the SGI Origin 2000 at the Division of Physics, Graduate School of Science, Hokkaido University, and on the VPP300/16R and VPP5000 at the Astronomical Data Analysis Center of the National Astronomical Observatory, Japan.

REFERENCES

Bahcall, N. A., Ostriker, J. P., Perlmutter, S., & Steinhardt, P. J. 1999, Science, 284, 1481
Bahcall, N. A., & Soneira, R. M. 1984, ApJ, 277, 27
Bertschinger, E. 1995, preprint (astro-ph/9506070)
Buote, D. A. 1998, MNRAS, 293, 381
Buote, D. A., & Tsai, J. C. 1995, ApJ, 452, 522
———. 1996, ApJ, 458, 27
Buote, D. A., & Xu, G. 1997, MNRAS, 284, 439
Clowe, D., Luppino, G. A., Kaiser, N., & Gioia, I. M. 2000, ApJ, 539, 540
Crone, M. M., Evrard A. E., & Richstone, D. O. 1996, ApJ, 467, 489
Davis, M., Efstathiou, G., Frenk, C. S., & White, S. D. M. 1985, ApJ, 292, 371
de Bernardis, P., et al. 2000, Nature, 404, 955
Dutta, S. N. 1995, MNRAS, 276, 1109
Ettori, S., Fabian, A. C., & White, D. A. 1997, MNRAS, 289, 787
Evrard, A. E., Mohr, J. J., Fabricant, D. G., & Geller, M. J. 1993, ApJ, 419, L9
Frenk, C. S., et al. 1999, ApJ, 525, 554
Gibson, B. K., et al. 2000, ApJ, 529, 723
Hernquist, L., & Katz, N. 1989, ApJS, 70, 419
Hockney, R. W., & Eastwood, J. W. 1981, Computer Simulation Using Particles (New York: McGraw-Hill)
Jing, Y. P., & Fang, L. Z. 1994, ApJ, 432, 438
Jing, Y. P., Mo, H. J., Börner, G., & Fang, L. Z. 1995, MNRAS, 276, 417
Luppino, G. A., & Kaiser, N. 1997, ApJ, 475, 20
Mellier, Y. 1999, ARA&A, 37, 127
Mohr, J. J., Evrard, A. E., Fabricant, D. G., & Geller, M. J. 1995, ApJ, 447, 8
Monaghan, J. J. 1992, ARA&A, 30, 543
Perlmutter, S., et al. 1999, ApJ, 517, 565
Press, W. H., Flannery, B. P., Teukolsky, S. A., & Vetterling, W. T. 1988, Numerical Recipes in C (Cambridge: Cambridge Univ. Press)
Richstone, D., Loeb, A., & Turner, E. L. 1992, ApJ, 393, 477
Riess, A. G., et al. 1998, AJ, 116, 1009
Schneider, P., & Bartelmann, M. 1997, MNRAS, 286, 696
Schuecker, P., Böhringer, H., Reiprich, T. H., & Feretti, L. 2001, A&A, 378, 408
Thomas, P. A., et al. 1998, MNRAS, 296, 1061
Totani, T., & Kobayashi, C. 1999, ApJ, 526, L65
Tsai, J. C., & Buote, D. A. 1996, MNRAS, 282, 77
Valdarnini, R., Ghizzardi, S., & Bonometto, S. 1999, NewA, 4, 71
Wilson, G., Cole, S., & Frenk, C. S. 1996, MNRAS, 282, 501
Yoshikawa, K., Jing, Y. P., & Suto, Y. 2000, ApJ, 535, 593